Entropy-driven phases at high coverage adsorption of straight rigid rods on two-dimensional square lattices

P. M. Pasinetti and A. J. Ramirez-Pastor*
Departamento de Física, Instituto de Física Aplicada (INFAP), Universidad Nacional de San Luis–CONICET, Ejército de Los Andes 950, D5700HHW, San Luis, Argentina

E. E. Vogel
Departamento de Física, Universidad de La Frontera, Casilla 54-D, Temuco 481180, Chile and Center for the Development of Nanoscience and Nanotechnology (CEDENNA), 9170124 Santiago, Chile

G. Saravia
Los Eucaliptus 1189, Temuco 4812537, Chile

(Received 27 August 2021; revised 7 November 2021; accepted 12 November 2021; published 29 November 2021)

Polymers are frequently deposited on different surfaces, which has attracted the attention of scientists from different viewpoints. In the present approach polymers are represented by rigid rods of length k (k-mers), and the substrate takes the form of an $L \times L$ square lattice whose lattice constant matches exactly the interspacing between consecutive elements of the k-mer chain. We briefly review the classical description of the nematic transition presented by this system for $k \geqslant 7$ observing that the high-coverage (θ) transition deserves a more careful analysis from the entropy point of view. We present a possible viewpoint for this analysis that justifies the phase transitions. Moreover, we perform Monte Carlo (MC) simulations in the grand canonical ensemble, supplemented by thermodynamic integration, to first calculate the configurational entropy of the adsorbed phase as a function of the coverage, and then to explore the different phases (and orientational transitions) that appear on the surface with increasing the density of adsorbed k-mers. In the limit of $\theta \to 1$ (full coverage) the configurational entropy is obtained for values of k ranging between 2 and 10. MC data are discussed in comparison with recent analytical results [D. Dhar and R. Rajesh, Phys. Rev. E **103**, 042130 (2021)]. The comparative study allows us to establish the applicability range of the theoretical predictions. Finally, the structure of the high-coverage phase is characterized in terms of the statistics of $k \times l$ domains (domains of l parallel k-mers adsorbed on the surface). A distribution of finite values of l ($l \ll L$) is found with a predominance of $k \times 1$ (single k-mers) and $k \times k$ domains. The distribution is the same in each lattice direction, confirming that at high density the adsorbed phase goes to a state with mixed orientations and no orientational preference. An order parameter measuring the number of $k \times k$ domains in the adsorbed layer is introduced.

DOI: 10.1103/PhysRevE.104.054136

I. INTRODUCTION

The study of systems of particles interacting with only excluded volume interactions has become an important topic in statistical mechanics, with applications to equilibrium and nonequilibrium systems. In equilibrium statistical mechanics, hard-sphere systems have been used to mimic phase transitions in molecular solids [1–3] and in colloidal crystals [4]. Other examples, corresponding to phase transitions in hard-sphere systems, can be found in [5–7]. On the other hand, systems of nonspherical hard objects have also been studied, showing that particle shape anisotropy can be a sufficient condition to induce the different phases (nematic, smectic, and cholestic) and phase transitions found in liquid crystals [8–14]. In nonequilibrium statistical mechanics, excluded volume models provide prototypical models for driven systems and jamming in granular systems [15–17].

In the case of lattice models of hard-core particles, the study of the phases of assemblies of particles of many different shapes has received considerable interest in the literature. The inherent complexity of the system still represents a major difficulty in the development of exact solutions, and only the hard hexagons model has been exactly solved [18]. In this context, approximate analytical procedures and Monte Carlo (MC) simulations have been used to study several particle shapes and their mixtures: Triangles [19], squares [20–26], dimers [27–32], mixtures of squares and dimers [33,34], Y-shaped particles [35–37], tetrominoes [38,39], rods [40–57], rectangles [45,58–60], and disks [61,62]. Experimental realizations of such systems include tobacco mosaic virus [63,64], liquid crystals [12], fd virus [65–67], silica colloids [68,69], boehmite particles [70,71], and DNA origami nanoneedles [72], as well as simple models for studying adsorption of molecules onto 2D substrates [73–75].

Systems of hard rods and cylinders have attracted a great deal of interest for many years. In a pioneer work, Onsager [76] predicted that very long and thin rods interacting with only excluded-volume interaction can lead to long-range

*To whom correspondence should be addressed: antorami@unsl.edu.ar

orientational (nematic) order. The nematic phase, characterized by a big domain of parallel molecules, is separated from an isotropic state by a phase transition occurring at a finite critical density depending on the length of the needle. For the lattice problem (which is the topic of this paper), the study of linear $k \times 1$ hard rods (or straight rigid k-mers) started with the work of Flory [77] and Zwanzig [78]. The model assumes that the rods can orient only in one of the d directions of a d-dimensional hypercubic lattice. In this line, a system of straight rigid k-mers on a square lattice, with two allowed orientations, was studied in Ref. [40]. Based on MC simulations, the authors presented strong numerical evidence that the system shows nematic order at intermediate densities for $k \geqslant 7$, over a critical density θ_{1c}. In addition, by means of high-density expansions, Ghosh and Dhar [40] provided a qualitative description of a second phase transition from a nematic order to a nonnematic state occurring at a critical density $\theta_{2c} \propto 1 - k^{-2}$ for large k.

Based on the seminal work of Ghosh and Dhar [40], several papers were devoted to the detailed study of the transitions occurring in a system of long straight rigid rods on 2D lattices with discrete allowed orientations [41–43,50–56]. In these articles, it was shown that, for $k < k_{\min}$, there is no phase transition, but for $k \geqslant k_{\min}$, as density is increased, there are three phases: a low-density disordered (isotropic) phase, an intermediate-density nematic phase, and a high-density phase in which there is no orientational order. The value of $k_{\min}$ depends on the lattice geometry, being $k_{\min} = 7$ for square [40,41] and triangular [42] lattices and $k_{\min} = 11$ for honeycomb [43] lattices. The intermediate-density nematic phase, characterized by a big domain of parallel k-mers, is separated from the low-density disordered state by a continuous transition at a finite critical density θ_{1c}. This first transition, usually referred to as an isotropic-nematic (I-N) phase transition, belongs to the 2D Ising universality class for square lattices [41] and the three-state Potts universality class for triangular [41] and honeycomb [43] lattices. In the three cases (square, triangular, and honeycomb lattices), the critical density characterizing the I-N transition θ_{1c} follows a power law as $\theta_{1c}(k) \propto k^{-1}$ [42]. The existence of the first transition was rigorously proved [56].

The relaxation time increases very quickly as the density increases. Consequently, usual MC simulations with local deposition-evaporation moves are very time consuming at high density and produce artifacts related to nonaccurate equilibrium states. In order to cope with these difficulties, efficient MC simulations based on cluster moves were developed in Refs. [50,51]. The use of these techniques has made it possible to investigate the behavior of the system at high densities. In this regime, a second phase transition from the intermediate-density nematic phase to the high-density phase has been reported [41,51]. The nature of this phase transition is not yet clear. There is some indication of the high-density phase having power-law correlations [51] with the second transition not being in the Ising universality class [51,52], while the exact solution of soft repulsive rods on a treelike lattice [53] suggests otherwise. The orientational transitions in two dimensions have also been studied using measures such as the classical entanglement entropy, mutability, Shannon entropy, and data compression [52,54,55].

Very recently, the asymptotic behavior of the entropy per site of full coverings of a $L \times M$ square lattice by straight rigid rods of length k was investigated [79]. The authors found that full coverage is possible only if at least one of L and M is a multiple of k, and that all allowed configurations can be reached from a standard configuration of all rods being parallel, using only basic flip moves that replace a $k \times k$ square of parallel horizontal rods by vertical rods, and vice versa. In addition, by combining the lower [79] and upper [80] bounds obtained for entropy, Dhar and Rajesh showed that, in the limit of large k, the configurational entropy per site tends to $Ak^{-2} \ln k$, with $A = 1$. Finally, based on a perturbative series expansion, the authors conjectured that the large-k behavior of entropy per site is superuniversal and continues to hold on d-dimensional hypercubical lattices for all $d \geqslant 2$. For low and intermediate coverage, the configurational entropy per site for a system of k-mers on square lattices has also been calculated [81–83].

The study of monodispersed hard rods of length k has also been investigated in three dimensions (simple cubic lattices) [84,85]. For $k \leqslant 4$, the system is disordered at all densities. For $k \geqslant 7$, three density-driven transitions are observed numerically: isotropic to nematic to layered-nematic to layered-disordered. In the layered-nematic phase, the system breaks up into layers, with nematic order in each layer, but very weak correlation between the ordering directions of different layers. In Ref. [84] the authors argue that the layered-nematic phase is a finite-size effect, and in the thermodynamic limit, the nematic phase will have higher entropy per site. For $4 < k < 7$, there is no nematic phase and a single phase transition from a disordered to a layered disordered phase [84,85].

Despite a long history, several basic questions about these systems remain open. Most of the unknown is in regard to the high-coverage phase, which has been less studied than the low and intermediate phases. What is the exact nature of the nonnematic phase that appears at high coverage? Is this phase present even when the density saturates in full coverage? How much of these results are algorithm induced? In this paper, we attempt to give at least partial answers to these questions discussing other features presented by these interesting systems. For this purpose, extensive MC simulations supplemented by the thermodynamic integration method have been used to calculate the configurational entropy per site of the adsorbed phase $s(k, \theta)$ as a function of coverage ($0 \leqslant \theta \leqslant 1$); the process has been done for different k-mer sizes ($2 \leqslant k \leqslant 10$). By comparing $s(k, \theta)$ with the configurational entropy per site corresponding to a fully aligned system (whose calculation reduces to the 1D case), the different phase transitions that occur on the surface were identified. The results obtained for θ close to 1 allowed us to test the recent theoretical predictions by Dhar and Rajesh [79]. The study of the high-coverage phase was completed by obtaining a basic statistics of domains of the l consecutive parallel k-mers adsorbed on the surface. The histograms measuring the accumulated frequencies of the $k \times l$ domains revealed the presence of finite domains (l much less than the lattice side) with a predominance of two characteristic lengths $l = 1$ and $l = k$. Based on these results, an order parameter measuring the number of $k \times k$ domains in the adsorbed layer has been introduced.

This paper is organized as follows. The calculation methodology is presented in Sec. II. The results are presented in the form of plots, which are discussed in Sec. III. The conclusions are summarized in Sec. IV.

II. METHODOLOGY: FUNCTIONS AND VARIABLES

A. Simulations: Adsorption-desorption algorithm

Lattice gas simulations of rods of length k (linear k-mers) were done in the grand canonical ensemble using the efficient algorithm presented by Kundu *et al.* [50,51], which was designed to overcome the slow sampling at high coverage. The temperature, T, chemical potential, μ, and system size, L, are kept fixed, whereas the number of particles, N, is allowed to fluctuate through nonlocal changes, i.e., insertion and/or remotion of several k-mers at the time (in contrast to the standard Metropolis algorithm).

In short, given a particular configuration of k-mers on the lattice, a Monte Carlo step (MCs) consists first in the removal of all the horizontal k-mers, keeping the vertical ones. In this way, each row consists in intervals of different length formed by contiguous empty sites. Such intervals are separated from each other by sites occupied by vertical k-mers.

Each interval, independently, could be filled by new horizontal k-mers, provided that its length be greater or equal to k. Given one of these intervals of length l ($\geqslant k$), it is very simple to calculate the equilibrium probability (given the temperature and chemical potential) of having the first k site of the interval occupied by an horizontal k-mer. Such probability could be precalculated and stored, for intervals of different lengths (from 0 to L) to increase the computational performance. From these probabilities it is possible to fill all the horizontal intervals of the system with new equilibrium configurations of horizontal k-mers and empty sites. The MCs is completed by repeating an identical procedure but emptying vertical intervals and refilling them with vertical k-mers.

In addition to the just described removal and filling processes of horizontal and vertical k-mers, it is found that the sampling and equilibrating times can be considerably reduced by adding patch or tile rotation steps. In this process, a site (i, j) is randomly selected. If that site is occupied by a head of an horizontal k-mer (i.e., its left-end site), we proceed to verify if the sites $(i, j+1)$, $(i, j+2)$,..., $(i, j+k-1)$ are also occupied by heads of horizontal k-mers. If so, we are in presence of a turnable patch consisting of k horizontal k-mers, which is replaced by a patch of k vertical k-mers. In the same way, we could have started with a vertical patch and turned it into a horizontal patch.

Then the complete MCs will consist of the remotion and filling processes, both horizontally and vertically, followed by the patch rotation process, which will be repeated a number of times equal to L^2, i.e., one per site in average. A detailed discussion can be found in the original works in Refs. [50,51]. The algorithm thus defined is proved to be ergodic and to satisfy the detailed balance principle.

The equilibrium is reached typically after $r_0 = 10^7$ MCs. A square lattice of $M = L^2$ sites with periodic border conditions was used. The relation L/k was fixed to 120, so that the finite-size effects can be neglected. The different observables of interest were obtained along other $r = 10^7$ configurations, i.e., the temporal series of the different order parameters as well as the average values obtained from these series.

B. Configurational entropy of the adsorbed phase: Thermodynamic integration method

The advantages of using MC simulations to calculate thermal averages of thermodynamic observables are well known [86,87]. The estimation of certain quantities such as the total energy, energy fluctuations, correlation functions, etc., is rather straightforward from averaging over a large enough number of instantaneous configurations (states) of a thermodynamic system. However, free energy and entropy are much more difficult to evaluate, and they cannot be directly computed. To calculate free energy and entropy, various methods have been developed [87]. Among them, the thermodynamic integration method is one of the most widely used and practically applicable [81,82,88–90].

In the grand canonical ensemble, the thermodynamic integration method relies upon integration of the chemical potential μ on coverage along a reversible path between an arbitrary reference state and the desired state of the system. This calculation also requires the knowledge of the total energy U for each obtained coverage. Thus, for a system made of N particles on M lattice sites, we have

$$\mu = \left(\frac{\partial F}{\partial N}\right)_{M,T}, \tag{1}$$

where $F = U - TS$ is the Helmholtz free energy and S is the configurational entropy. It follows that

$$S(k, M, N, T) = S_0(k, M, N_0, T) + \frac{U(k, M, N, T) - U(k, M, N_0, T)}{T} - \frac{1}{T}\int_{N_0}^{N} \mu dN. \tag{2}$$

In our case $U(k, M, N, T) = 0$ and the determination of the entropy in the reference state, $S_0(k, M, N_0, T)$, is trivial [$S_0(k, M, N_0, T) = 0$ for $N_0 = 0$]. Then, after writing the last equation in terms of intensive variables, the configurational entropy per site ($s = S/M$) results in

$$\frac{s(k, \theta, T)}{k_B} = -\frac{1}{k_B T}\int_0^{\theta} \frac{\mu}{k}\, d\theta, \tag{3}$$

where $\theta = kN/M$ and k_B is the Boltzmann constant. Given that all chemical potentials are being measured in units of $k_B T$, all results will be independent of the temperature. Accordingly, for the rest of the paper we will use $s(k, \theta)$ to denote the configurational entropy per site (for simplicity we will drop the "T").

The curve of μ vs θ can be obtained by following the adsorption-desorption algorithm described in Sec. II A. In our MC simulations, we varied the chemical potential and monitored the density θ, which can be calculated as a simple average:

$$\theta = \frac{k\langle N\rangle}{M}, \tag{4}$$

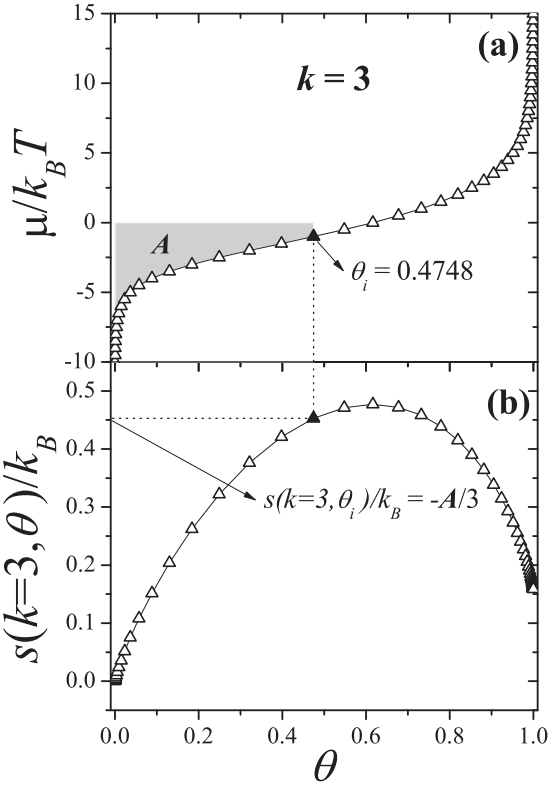

FIG. 1. Chemical potential (a) and configurational entropy per site (b) as function of coverage for $k = 3$. The figure illustrates the implementation of the thermodynamic integration method. The value of A is -1.3586. The adsorption isotherm in (a) was measured in the range from $\mu/k_BT = -15$ to $\mu/k_BT = 25$. A shorter range is shown ($-10 \leqslant \mu/k_BT \leqslant 15$) for a better visualization.

where the brackets $\langle\cdot\rangle$ denote the average over the r MC simulation runs after equilibrium is settled.

In order to illustrate the implementation of the methodology, an example corresponding to $k = 3$ is shown in Fig. 1. In Fig. 1(a) the curve $\mu(\theta)$ is reported. The error bars are smaller than the size of the symbols, which tells the accuracy of the simulated data. To apply the method, a given point θ_i is chosen, and the integral $A = \int_0^{\theta_i} (\mu/k_BT)\, d\theta$ is calculated. In the figure, $\theta_i = 0.4748$ (solid triangle) and $A = -1.3586$. The corresponding entropy per site yields $s(k = 3, \theta_i)/k_B = -A/3 = 0.4529$ [see solid triangle in Fig. 1(b)]. By repeating the procedure for all values of θ_i, the curve of entropy vs coverage can be calculated.

The integration required in Eq. (3) is carried out using the well-known trapezoidal rule [91]. Accordingly, two error sources affect the entropy calculations: (1) the simulation error associated with the measurement of the adsorption isotherm and (2) the error inherent to the integration method. With respect to the simulation error, each point in the adsorption isotherm curve is obtained with an error of the order of 10^{-5}. Then, since the integral A is calculated by summing over all points of the adsorption isotherm between $\theta \approx 0$ and $\theta = \theta_i$ [91], the resulting simulation error for A increases with the coverage. On the other hand, the error coming from the integration method can be controlled by choosing appropriately the number of integration points n_μ (number of discrete values in the adsorption isotherm) [91]. In the present study, the choice of n_μ is made such that the integration error is much smaller than the simulation error.

The complete range of integration extends from $\mu/k_BT = -15$ ($\theta \approx 0$) to $\mu/k_BT = 25$ ($\theta \approx 1$); our main interest is precisely in the approach to this upper limit. Such interval is covered upon increasing μ/k_BT in intervals of 0.5, thus defining curves with $n_\mu = 81$ points. With these values for the parameters, the simulation error is of the order of 10^{-3}, and the integration error is negligible with respect to the simulation error. All of this leads to the total error for the entropy per site at full coverage that will be reported in the next section (see the sixth column in Table I below).

III. RESULTS AND DISCUSSION

The phase properties of systems with purely steric interactions are important from a statistical mechanical perspective because the potential energy, U, of a steric system is, by definition, constant. Consequently, the Helmholtz free energy

TABLE I. Configurational entropy per site for straight rigid rods on square lattices (at full coverage) with k in the range [2,10]. First column, k-mer size k; second column, lower bound for entropy per site obtained by solving exactly a system of rods on semi-infinite strips $k \times \infty$ [79]; third column, same as second column but for semi-infinite strips $2k \times \infty$ [79]; fourth column, upper bound for entropy per site obtained in Ref. [80]; fifth column, theoretical predictions from Eq. (6) (the values are rounded to five decimal places) [79]; sixth column, MC results obtained in the present work, where statistical errors are in the last digit and are indicated in parentheses; and seventh column, relative differences between theoretical data in fifth column and MC results in sixth column (see definition in the text).

	Entropy per site at full coverage, $s(k, \theta = 1)/k_B$					
k	Strips $k \times \infty$ [79]	Strips $2k \times \infty$ [79]	Upper bound [80]	Eq. (6) [79]	MC results (this work)	δ
2	0.2406059	0.2609982	0.2915677	0.17329	0.293(2)	0.409
3	0.1274150	0.1410668	0.1746373	0.12207	0.159(2)	0.232
4	0.0805712	0.0899073	0.1162136	0.08664	0.101(2)	0.142
5	0.0562399	0.0629820	0.0833025	0.06438	0.070(3)	0.080
6	0.0418189	0.0469143	0.0629134	0.04977	0.052(3)	0.043
7	0.0324961	0.0364864	0.0493680	0.03971	0.040(3)	0.007
8	0.0260854	0.0292992	0.0398838	0.03249	0.032(3)	0.015
9	0.0214689	0.0241160	0.0329673	0.02713	0.027(3)	0.005
10	0.0180229	0.0202437	0.0277571	0.02303	0.021(3)	0.095

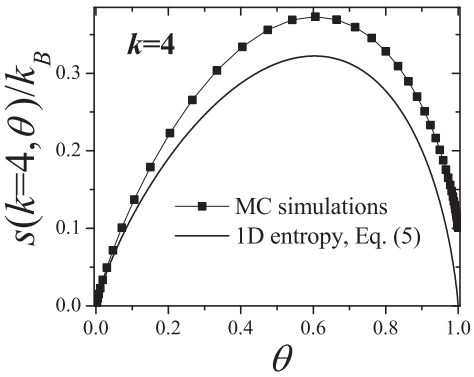

FIG. 2. Configurational entropy per site as function of coverage comparing simulations (symbols) and theory (solid line) according to expression in Eq. (5). The values have been obtained for $k = 4$.

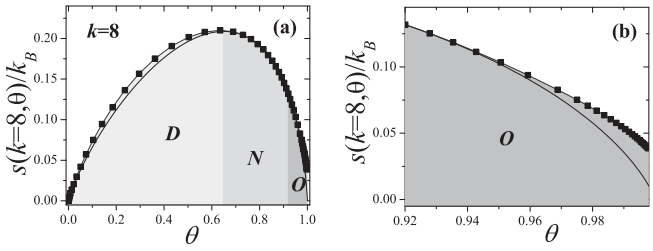

FIG. 3. (a) Same as Fig. 2 but for $k = 8$. (b) The departure of the theoretical expression [Eq. (5), solid line] from simulations (symbols) at high coverage.

$F = U - TS$ is controlled by entropy (S) alone, and all phase transitions are entropy driven. In this way, the behavior of entropy as a function of coverage appears as a useful property to explore the possible ordered phases present in these systems for increasing values of the density.

As established in previous works [40,41] the system does not present long-range order at all densities for $k < 7$. This can be visualized for $k = 4$ in Fig. 2, where the configurational entropy per site obtained by the thermodynamic integration method (symbols) is compared with the configurational entropy per site obtained analytically for a fully aligned system (line). In the fully aligned or nematic state, the system would be characterized by a big domain of parallel k-mers (tetramers in the case of Fig. 2), and the entropy of this nematic state having density θ can be reduced to the entropy of a 1D problem [92]:

$$\frac{s_{1D}(k,\theta)}{k_B} = \left[1 - \frac{(k-1)}{k}\theta\right] \ln\left[1 - \frac{(k-1)}{k}\theta\right] - \frac{\theta}{k}\ln\frac{\theta}{k} - (1-\theta)\ln(1-\theta). \quad (5)$$

As observed in Fig. 2, the aligned system has smaller entropy over the entire range of coverage. This finding indicates that, in the case of $k = 4$ and according to the principle of maximum entropy, the adsorbed phase does not reach nematic order at any point when the density varies between 0 and 1.

The behavior of these systems becomes more interesting for $k \geqslant 7$ [40,41]. When this condition is satisfied, the adsorbed phase shows nematic order at intermediate and high densities, and goes to a state with mixed orientations at very high density where the long-range orientational order is lost. The high-density phase is characterized by the formation of local arrangements (or islands) of parallel k-mers. Next, this picture will be analyzed in terms of entropy.

In Fig. 3(a) the configurational entropy per site has been studied for a system with $k = 8$. Symbols represent MC simulation data, and the solid line corresponds to the analytical exact entropy corresponding to a fully aligned state [Eq. (5) with $k = 8$].

For low coverage, the systems present no order, and, accordingly, the true 2D entropy is higher than that from Eq. (5). At intermediate densities, there exists a range of densities for which the system is characterized by a big domain of parallel k-mers and the configurational entropy per site can be well approximated by Eq. (5). In this range, the nematic order is almost perfect (the number of nonaligned k-mers is negligible), and, accordingly, simulation and theoretical curves are practically overlapping (within the statistical errors). This result provides a physical interpretation of the I-N transition occurring in the system, showing that it is more favorable for the k-mers to align spontaneously, since the resulting loss of orientational entropy is by far compensated by the gain of translational entropy. Finally, as the coverage approaches 1, the configurational entropy of the 2D system departs from the corresponding one to the nematic phase, indicating the loss of orientational order in the adsorbed phase [see Fig. 3(b)].

The value of the critical density associated with the I-N phase transition, θ_{1c}, can be estimated from the minimum value of θ which occurs the near superposition of the 1D and 2D data. The coverage where the two curves separate should be indicative of the critical density corresponding to the N-O phase transition, θ_{2c}. However, it is important to emphasize that the calculation of the entropy of the nematic phase from the 1D model is an approximation (especially in the region near the critical densities, where the phase is not completely aligned). Consequently, a precise determination of θ_{1c} and θ_{2c} requires an extensive work based on MC simulations and finite-size scaling techniques [42,54,55]. In the case of Fig. 3(a), the border regions vary between 0.62 and 0.68 (I-N), and between 0.89 and 0.95 (N-O). The values of θ_{1c} and $\theta_{2,c}$ previously obtained in the literature for $k = 8$ are $\theta_{1,c} \approx 0.643$ [42,54] and $\theta_{2,c} \approx 0.92$ [55].

Schematic representations of the different phases that appear on increasing the density are shown in Fig. 4: Fig. 4(a) the disordered-isotropic phase, D region in Fig. 3(a); Fig. 4(b) the nematic phase, N region in Fig. 3(a); and Fig. 4(c) the ordered-isotropic phase, O region in Fig. 3(a). In spite that the results reported here were obtained for $L/k = 120$, we have chosen $L/k = 10$ (and $k = 8$) for clarity in Fig. 4.

D and N phases have been well studied and characterized [40]. The same has not happened so far for the case of the O phase. In the limit case of $\theta \to 1$, Dhar and Rajesh [79] recently showed that the configurational entropy per site of fully packed k-mers on d-dimensional hypercubic lattices follows the law

$$\frac{s(k,\theta=1)}{k_B} = k^{-2}\ln k \quad (k \to \infty). \quad (6)$$

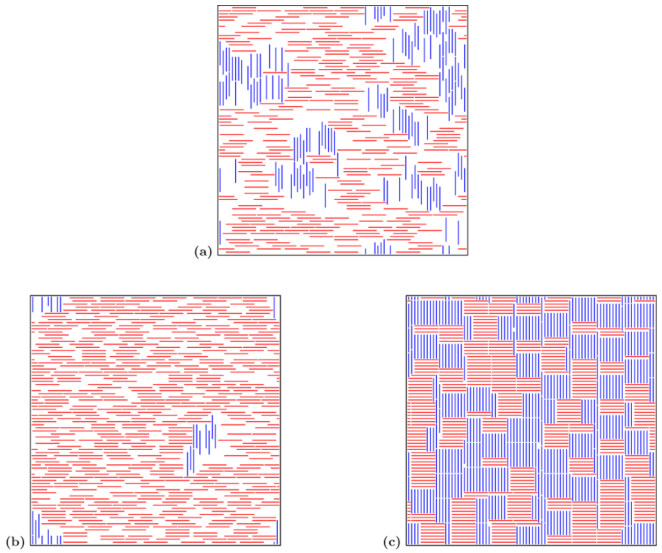

FIG. 4. (a) Snapshot for an example of a disordered-isotropic phase [D region in Fig. 3(a)]. (b) Snapshot for an example of a nematic phase [N region in Fig. 3(a)]. (c) Snapshot for an example of an ordered-isotropic phase [O region in Fig. 3(a)]. The configurations shown in (a)–(c) have been obtained for square lattices with $k = 8$ and $L/k = 10$, which are appropriate for illustrative purposes.

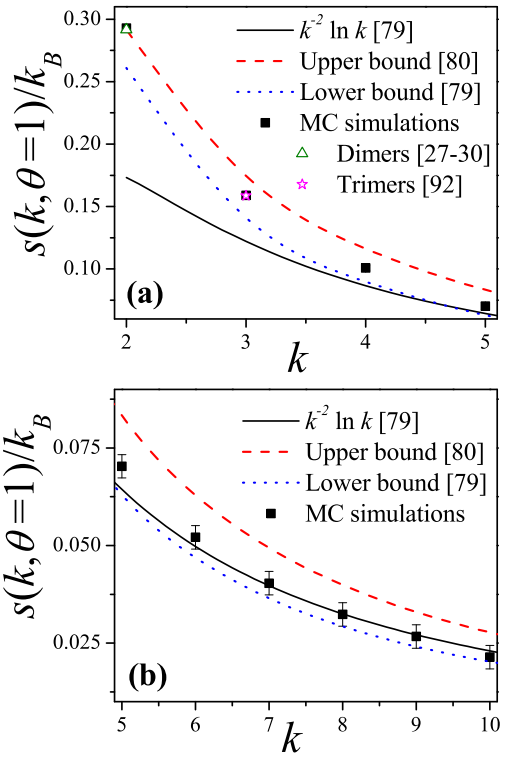

FIG. 5. Configurational entropy per site at full coverage ($\theta = 1$) as a function of k: (a) $2 \leqslant k \leqslant 5$ and (b) $5 \leqslant k \leqslant 10$. Solid squares correspond to MC simulation data (this work). The open triangle and open star represent theoretical values obtained for dimers [27–30] and trimers [93], respectively. The solid line indicates results obtained from Eq. (6) [79]. The lower bound (third column in Table I, Ref. [79]) is denoted by the dotted line, while the upper bound (fourth column in Table I, Ref. [80]) is denoted by the dashed line.

Based on a perturbative series expansion, the authors conjectured that Eq. (6) holds for all $d \geqslant 2$.

Equation (6) has not been corroborated yet by MC methods. As is well known, the relaxation time increases very quickly as the density increases, and, consequently, MC simulations at high density are very time consuming and may produce artifacts related to inaccurate equilibrium states. With these ideas in mind, exhaustive MC simulations supplemented by the thermodynamic integration method were developed here to calculate $s(k, \theta \to 1)/k_B$. In the calculations, the curve of $\mu(\theta)$ was integrated following the procedure described in Sec. II. The results are shown in Fig. 5. Solid squares represent MC results, and the solid line corresponds to Eq. (6). Numerical and theoretical values are also compiled in Table I.

Figure 5 also includes two theoretical bound curves. The lower bound (dotted line) was obtained by solving exactly the entropy per site of rods on semi-infinite strips $2k \times \infty$ [79]. The corresponding numerical values are shown in Table I (third column). In Ref. [79] the entropy per site at full coverage was also calculated for semi-infinite strips $k \times \infty$. The obtained values are compiled in the second column of Table I but are not shown in Fig. 5. On the other hand, the upper bound (dashed line) represents the result obtained by Gagunashvili and Priezzhev [80] for the entropy on the square lattice: $s(k, \theta = 1)/k_B \leqslant k^{-2} \ln(\gamma k)$, where $\gamma = \exp(4G/\pi)/2$ and $G = 0.91596\ldots$ is Catalan's constant. The numerical data corresponding to the upper bound curve in Fig. 5 are collected in Table I (fourth column).

The data in Fig. 5 were divided in two parts for a better visualization. In Fig. 5(a) the curves are plotted in the range $2 \leqslant k \leqslant 5$. Significant differences are observed between MC data (which remain between the two bound curves) and theoretical results from Eq. (6). For the case of dimers ($k = 2$), the entropy per site for the square lattice has been exactly calculated, $s(k = 2, \theta = 1)/k_B = G/\pi = 0.29156\ldots$ [27–30]. The exact value in Refs. [27–30] coincides with the value of the upper bound for $k = 2$: $2^{-2} \ln(2\gamma) = 2^{-2}(4G/\pi) = G/\pi$. In addition, a precise estimate $s(k = 3, \theta = 1)/k_B = 0.158520(15)$ has been obtained for trimers on square lattices [93]. The theoretical values for $k = 2$ and 3 agree, within the statistical errors, with those obtained here by MC simulations. See the fifth column in Table I and Fig. 5(a): dimers (open triangle) and trimers (open star). In Fig. 5(a) the error bars are smaller than the size of the symbols. The perfect agreement between previous and current results validates our computational approach and calculation method.

As the k-mer size increases [see Fig. 5(b) where the data are presented in the range $5 \leqslant k \leqslant 10$], the differences between the MC values and those predicted by Eq. (6) diminish. This effect can be easily rationalized with the help of the relative difference δ, which is defined as $|s_{MC} - s_{\text{theo}}|/s_{MC}$, where s_{MC} denotes the simulation data (sixth column in Table I) and s_{theo} represents theoretical data from Eq. (6) (fifth column in Table I). The relative differences are collected in the seventh column of Table I. For $k \geqslant 6$, these differences are less than the relative simulation errors. In other words, theoretical and simulation results coincide, within the statistical uncertainty, in the range $k \geqslant 6$. Note, in addition, that the Dhar and Rajesh

curve falls between the upper and lower bounds for $k \geqslant 5$. These findings represent the first numerical validation of the expression obtained in Ref. [79] and allows for an accurate determination of of its validity range.

In addition to analyzing the entropy, it is also interesting to be able to characterize the structure of the O phase. For this purpose, and following the scheme of Dhar and Rajesh [79], the study will be restricted to fully occupied lattices. As shown in Fig. 4(c), the high-density phase is characterized by the formation of $k \times l$ domains of parallel k-mers (with variable l). These domains are randomly oriented so that the O phase has no net orientational order.

The length l of a domain is somewhat difficult to define since pure $k \times l$ domains are hard to be found near saturation density as can be appreciated from Fig. 4(c). We counted all the perfect domains with length k and length l. When there is an discontinuity due to the shift of even just one k-mer the count for a new domain begins. This is the simplest possible way of measuring l, but it certainly biases the measure in favor of shorter l values. Take, for instance, the domain of vertical k-mers in the upper part of Fig. 4(c), beginning about $L/3$ from the left margin: the width is $k = 8$ with five initial vertical k-mers ($l_1 = 5$), then there are two shifted single bars. How do we count them? Then the original domain seems to continue beyond this break with a tile $k \times k$; again we see single vertical bars followed by another $k \times k$ domain, which bifurcates returning to the left margin via periodic boundary conditions. What is the effective l for this domain? No unique way of answering this question is in sight. In spite of this shortcoming we go ahead and obtain histograms for $l(k)$ which can give insight into some of the properties of these domains.

The number of domains of length l has been measured in the simple way proposed above for a number n of equilibrium high coverage configurations. For each value of k, the apparition frequency of a domain of length l is denoted as $f_k(l)$:

$$f_k(l) = \frac{\text{total number of domains of length } l \text{ in the } n \text{ measured samples}}{\text{total number of domains in the } n \text{ measured samples}}. \tag{7}$$

In Fig. 6 the frequency $f_k(l)$ is shown (in a semilog scale) as a function of the length l for two different values of k: (a) $k = 4$, and (b) $k = 8$. The simulations were performed for $L/k = 120$. $r_0 = 10^6$ MCs were used to equilibrate the systems. Then the number of domains of length l was averaged over $n = 10^5$ independent configurations. The procedure was carried out for a very high value of the chemical potential ($\mu/k_BT = 20$), being the corresponding coverage close to 1 ($\theta \approx 0.998$). The results in the figure indicate that single k-mers (domains with $l = 1$) and $k \times k$ islands dominate the distributions. The procedure in Fig. 6 was repeated for $2 \leqslant k \leqslant 10$, always obtaining similar qualitative trends. In addition, identical histograms were obtained in each lattice direction, corroborating that the O phase has no net orientational preference.

The results obtained from the statistical analysis presented in Fig. 6 indicate that the high-coverage phase presents a short-range order leading to finite $k \times l$ domains with predominance of lengths $l = 1$ and $l = k$. Accordingly, the dependence on coverage (and k) of the number of $k \times k$ domains, or flippable blocks as they are called in Ref. [79], could be used to describe the transition occurring at high density. For this, it is more convenient to define the parameter ϕ as

$$\phi = \frac{\text{number of flippable } k \times k \text{ domains}}{(L/k)^2}, \tag{8}$$

where $(L/k)^2$ is a normalization term that ensures that ϕ varies between 0 and 1.

As an illustrative example, Fig. 7 shows the order parameter ϕ as function of coverage for straight rigid k-mers with $k = 8$ (and $L/k = 120$). When the system presents nematic order, the number of perfectly aligned k-mers is small [see Fig. 4(b)] and the order parameter is minimum. As the chemical potential is increased above a certain critical value, adsorbed k-mers form $k \times k$ structures and ϕ is different from zero. In the figure, the critical chemical potential is $\mu/k_BT \approx 8$. This value corresponds to a density $\theta \approx 0.94$, which is in the border between the N and O phases [see Fig. 3(b)].

The study presented in Fig. 7 shows that ϕ appears as a good order parameter, evidencing the phase transition occurring in the adsorbed layer at high density. Taking advantage

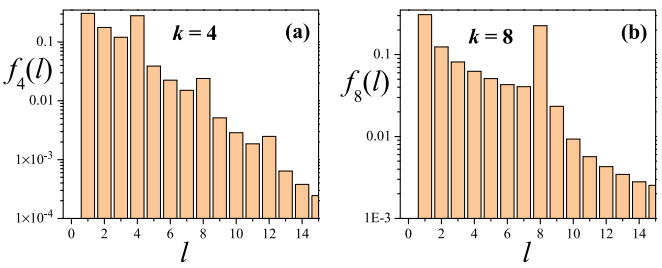

FIG. 6. (a) $f_k(l)$ as a function of the length l (see discussion in the text) for $k = 4$. (b) Same as (a) for $k = 8$.

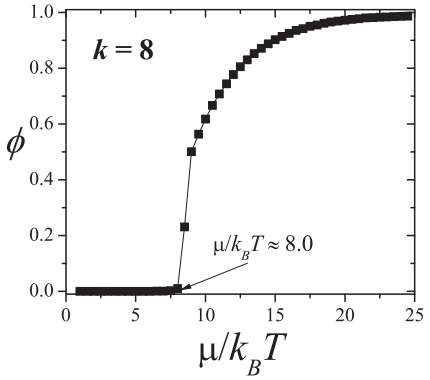

FIG. 7. Parameter ϕ [Eq. (8)] as function of coverage for straight rigid k-mers with $k = 8$.

of its definition (and related functions such as susceptibility, reduced fourth-order cumulant, etc.), a complete analysis of criticality and universality will be an object of future work.

IV. CONCLUSIONS

In the present work, we have addressed the critical properties of straight rigid rods adsorbed on square lattices. The process was mainly analyzed in terms of the configurational entropy of the adsorbed phase. The results were obtained by combining Monte Carlo simulations, the thermodynamic integration method, and theoretical analysis.

Special interest was devoted to the study of the high-coverage phase (O phase), which has been much less explored in the literature. Using MC simulations and the thermodynamic integration method, the behavior of the configurational entropy per site at full coverage as a function of the k-mer size was obtained and compared with the recently reported expression $s(k, \theta = 1)/k_B = k^{-2} \ln k$ $(k \to \infty)$ [79]. The MC study presented here represents, to our best knowledge, the first numerical validation of the theoretical predictions of Rajesh and Dhar [79]. The structure of the O phase was also investigated by analyzing the statistics of the $k \times l$ domains that occur in the adsorbed phase in the regime of high densities (close to 1). Based on this study (and previous research), the following conclusions can be drawn.

The high-coverage transition presented by systems with $k \geqslant 7$ is nothing but the recovery of the natural tendency of approaching a short-range ordering in the form of paths of width k; these paths occur randomly for all k values, in both horizontal and vertical directions, leading to nil results for the long-range orientational order parameter at high coverage.

This monotonic sequence is interrupted for $k \geqslant 7$ when a nematic transition occurs for $\theta \geqslant \theta_{1c}$ when an ergodicity breaking occurs and the system tends to present a preferred direction for subsequent depositions. This transition is entropy driven as large enough rods present more translational degrees of freedom leading to larger entropy. As coverage increases another form of entropy of no previous importance takes over: the relative distributions of domains with vertical or horizontal k-mers. Then the nematic phase is abandoned, and the system at $\theta \geqslant \theta_{2c}$ breaks into a system of short-range labyrinthine domains with mixed orientations.

As longer rods are considered, θ_{1c} moves to lower values while θ_{2c} moves to larger values, thus making the nematic phase wide in the range of θ. These critical densities behave differently, and θ_{2c} moves very fast to the saturation value 1.0. On the other hand, $\theta_{1c} \to 0$ at a slower rate with respect to k values.

The exact nature of the O phase cannot be obtained from entropic considerations, and it must relay in order parameters that reflect the new ordering. Obviously the long-range orientational order parameter is not appropriate for this purpose since it vanishes without being an indicator of the kind of new order reached. So this question will remain open because to answer it new parameters need to be defined, tested, measured, and interpreted. The parameter ϕ measuring the number of $k \times k$ domains in the adsorbed layer seems to be a promising way in this direction. This extensive computational work is at the moment beyond the scope of the present paper.

However, we can say that we expect the N phase to prevail near the saturation coverage for large enough k values, since the ergodicity breaking defining the N phase is favored for large k. At the same time, the O phase is pushed away quickly as $\theta_{2c} \to 1$ for large k values.

The way the configuration space is swept is likely to be determinant in the way the configurations at high coverage are found. The step in which $k \times k$ tiles are turned by 90° favors configurations with such structures in detriment of configurations with no such possibility. Thus, a random sampling of the configuration space, although needing huge computational times, could eventually produce histograms different from those reported in Fig. 6. But the entropy functions, handling logarithms of similar numbers, will differ only very slightly, and the discussions and general conclusions outlined above will still hold.

Future efforts will be done following two directions: (1) to extend the present analysis to other d-dimensional hypercubical lattices ($d \geqslant 2$), where the validity of Eq. (6) has been conjectured and has not yet been rigorously proved [79]; and (2) based on the definition of the parameter ϕ and other order parameters characterizing the O phase, to develop a complete finite-size scaling study of the phase transition occurring in the adsorbed layer at densities close to 1.

ACKNOWLEDGMENTS

This work was supported in part by CONICET (Argentina) under Project No. PIP 112-201101-00615; Universidad Nacional de San Luis (Argentina) under Project No. 03-1920; and CEDENNA (Chile) under Contract No. Conicyt AFB180001 and Fondecyt (Chile) under Contract No. 1190036. The numerical work was done using the BACO parallel cluster [94] located at the Instituto de Física Aplicada, Universidad Nacional de San Luis–CONICET, San Luis, Argentina.

[1] B. J. Alder and T. E. Wainwright, J. Chem. Phys. **27**, 1208 (1957).
[2] B. J. Alder and T. E. Wainwright, Phys. Rev. **127**, 359 (1962).
[3] E. G. Noya, C. Vega, and E. de Miguel, J. Chem. Phys. **128**, 154507 (2008).
[4] P. N. Pusey and W. van Megen, Nature (London) **320**, 340 (1986).
[5] P. W. Bridgman, Phys. Rev. **3**, 126 (1914).
[6] P. W. Bridgman, Phys. Rev. **3**, 153 (1914).
[7] O. K. Rice, J. Chem. Phys. **15**, 875 (1947).
[8] E. A. DiMarzio, J. Chem. Phys. **35**, 658 (1961).
[9] M. E. Fisher, J. Math. Phys. **7**, 1776 (1966).
[10] J. Vieillard-Baron, J. Chem. Phys. **56**, 4729 (1972).
[11] R. Möessner and S. L. Sondhi, Phys. Rev. B **68**, 054405 (2003).

[12] P.-G. de Gennes and J. Prost, *The Physics of Liquid Crystals* (Oxford University Press, New York, 1995).
[13] D. Frenkel, J. Phys. Chem. **92**, 3280 (1988).
[14] C. Care and D. Cleaver, Rep. Prog. Phys. **68**, 2665 (2005).
[15] A. Donev, S. Torquato, F. H. Stillinger, and R. Connelly, J. Appl. Phys. **95**, 989 (2004).
[16] T. M. Liggett, *Interacting Particle Systems*, Classics in Mathematics (Springer, New York, 2012), Vol. 276.
[17] K. Mallick, Physica A **418**, 17 (2015).
[18] R. J. Baxter, J. Phys. A **13**, L61 (1980).
[19] A. Verberkmoes and B. Nienhuis, Phys. Rev. Lett. **83**, 3986 (1999).
[20] A. Bellemans and R. K. Nigam, J. Chem. Phys. **46**, 2922 (1967).
[21] A. Bellemans and R. K. Nigam, Phys. Rev. Lett. **16**, 1038 (1966).
[22] F. H. Ree and D. A. Chesnut, J. Chem. Phys. **45**, 3983 (1966).
[23] K. Ramola and D. Dhar, Phys. Rev. E **86**, 031135 (2012).
[24] T. Nath, D. Dhar, and R. Rajesh, Europhys. Lett. **114**, 10003 (2016).
[25] T. Nath and R. Rajesh, J. Stat. Mech. (2016) 073203.
[26] D. Mandal, T. Nath, and R. Rajesh, J. Stat. Mech. (2017) 043201.
[27] P. Kasteleyn, Physica **27**, 1209 (1961).
[28] P. Kasteleyn, J. Math. Phys. **4**, 287 (1963).
[29] H. N. V. Temperley and M. E. Fisher, Philos. Mag. **6**, 1061 (1961).
[30] M. E. Fisher, Phys. Rev. **124**, 1664 (1961).
[31] O. J. Heilmann and E. H. Lieb, Commun. Math. Phys. **25**, 190 (1972).
[32] D. A. Huse, W. Krauth, R. Moessner, and S. L. Sondhi, Phys. Rev. Lett. **91**, 167004 (2003).
[33] K. Ramola, K. Damle, and D. Dhar, Phys. Rev. Lett. **114**, 190601 (2015).
[34] D. Mandal and R. Rajesh, Phys. Rev. E **96**, 012140 (2017).
[35] P. Szabelski, W. Rżysko, T. Panczyk, E. Ghijsens, K. Tahara, Y. Tobe, and S. De Feyter, RSC Adv. **3**, 25159 (2013).
[36] D. Ruth, R. Toral, D. Holz, J. Rickman, and J. Gunton, Thin Solid Films **597**, 188 (2015).
[37] D. Mandal, T. Nath, and R. Rajesh, Phys. Rev. E **97**, 032131 (2018).
[38] L. Mao, H. H. Harris, and K. J. Stine, J. Chem. Inf. Comput. Sci. **42**, 1179 (2002).
[39] B. C. Barnes, D. W. Siderius, and L. D. Gelb, Langmuir **25**, 6702 (2009).
[40] A. Ghosh and D. Dhar, Eur. Phys. Lett. **78**, 20003 (2007).
[41] D. A. Matoz-Fernandez, D. H. Linares, and A. J. Ramirez-Pastor, Eur. Phys. Lett. **82**, 50007 (2008).
[42] D. A. Matoz-Fernandez, D. H. Linares, and A. J. Ramirez-Pastor, J. Chem. Phys. **128**, 214902 (2008).
[43] D. A. Matoz-Fernandez, D. H. Linares, and A. J. Ramirez-Pastor, Physica A **387**, 6513 (2008).
[44] T. Fischer and R. L. C. Vink, Eur. Phys. Lett. **85**, 56003 (2009).
[45] J. Kundu and R. Rajesh, Phys. Rev. E **91**, 012105 (2015).
[46] P. Longone, D. H. Linares, and A. J. Ramirez-Pastor, J. Chem. Phys. **132**, 184701 (2010).
[47] P. Longone, M. Dávila, and A. J. Ramirez-Pastor, Phys. Rev. E **85**, 011136 (2012).
[48] P. Quiring, M. Klopotek, and M. Oettel, Phys. Rev. E **100**, 012707 (2019).
[49] D. H. Linares, F. Romá, and A. J. Ramirez-Pastor, J. Stat. Mech. (2008) P03013.
[50] J. Kundu, R. Rajesh, D. Dhar, and J. F. Stilck, AIP Conf. Proc. **1447**, 113 (2012).
[51] J. Kundu, R. Rajesh, D. Dhar, and J. F. Stilck, Phys. Rev. E **87**, 032103 (2013).
[52] C. Chatelain and A. Gendiar, Eur. Phys. J. B **93**, 134 (2020).
[53] J. Kundu and R. Rajesh, Phys. Rev. E **88**, 012134 (2013).
[54] E. E. Vogel, G. Saravia, and A. J. Ramirez-Pastor, Phys. Rev. E **96**, 062133 (2017).
[55] E. E. Vogel, G. Saravia, A. J. Ramirez-Pastor, and M. Pasinetti, Phys. Rev. E **101**, 022104 (2020).
[56] M. Disertori and A. Giuliani, Commun. Math. Phys. **323**, 143 (2013).
[57] D. Dhar, R. Rajesh, and J. F. Stilck, Phys. Rev. E **84**, 011140 (2011).
[58] J. Kundu and R. Rajesh, Phys. Rev. E **89**, 052124 (2014).
[59] T. Nath, J. Kundu, and R. Rajesh, J. Stat. Phys. **160**, 1173 (2015).
[60] P. Gurin, S. Varga, M. González-Pinto, Y. Martínez-Ratón, and E. Velasco, J. Chem. Phys. **146**, 134503 (2017).
[61] H. C. M. Fernandes, J. J. Arenzon, and Y. Levin, J. Chem. Phys. **126**, 114508 (2007).
[62] T. Nath and R. Rajesh, Phys. Rev. E **90**, 012120 (2014).
[63] X. Wen, R. B. Meyer, and D. L. D. Caspar, Phys. Rev. Lett. **63**, 2760 (1989).
[64] S. Fraden, G. Maret, D. L. D. Caspar, and R. B. Meyer, Phys. Rev. Lett. **63**, 2068 (1989).
[65] E. Grelet, Phys. Rev. Lett. **100**, 168301 (2008).
[66] Z. Dogic and S. Fraden, Phys. Rev. Lett. **78**, 2417 (1997).
[67] Z. Dogic and S. Fraden, Langmuir **16**, 7820 (2000).
[68] A. Kuijk, A. V. Blaaderen, and A. Imhof, J. Am. Chem. Soc. **133**, 2346 (2011).
[69] A. Kuijk, D. V. Byelov, A. V. Petukhov, A. V. Blaaderen, and A. Imhof, Faraday Discuss. **159**, 181 (2012).
[70] P. A. Buining and H. N. W. Lekkerkerker, J. Phys. Chem. **97**, 11510 (1993).
[71] M. P. B. van Bruggen, F. M. van der Kooij, and H. N. W. Lekkerkerker, J. Phys.: Condens. Matter **8**, 9451 (1996).
[72] A. Czogalla, D. J. Kauert, R. Seidel, P. Schwille, and E. P. Petrov, Nano Lett. **15**, 649 (2015).
[73] B. Dünweg, A. Milchev, and P. A. Rikvold, J. Chem. Phys. **94**, 3958 (1991).
[74] A. Patrykiejew, S. Sokolowski, and K. Binder, Surf. Sci. Rep. **37**, 207 (2000).
[75] S. Mitchell, G. Brown, and P. Rikvold, Surf. Sci. **471**, 125 (2001).
[76] L. Onsager, Ann. N.Y. Acad. Sci. **51**, 627 (1949).
[77] P. J. Flory, Proc. R. Soc. A **234**, 60 (1956).
[78] R. Zwanzig, J. Chem. Phys. **39**, 1714 (1963).
[79] D. Dhar and R. Rajesh, Phys. Rev. E **103**, 042130 (2021).
[80] N. D. Gagunashvili and V. B. Priezzhev, Theor. Math. Phys. **39**, 507 (1979).
[81] F. Romá, A. J. Ramirez-Pastor, and J. L. Riccardo, J. Chem. Phys. **114**, 10932 (2001).
[82] F. Romá, A. J. Ramirez-Pastor, and J. L. Riccardo, Langmuir **16**, 9406 (2000).
[83] D. V. Kokosinskii and M. V. Ulyanov, J. Phys.: Conf. Ser. **1740**, 012015 (2021).

[84] N. Vigneshwar, D. Dhar, and R. Rajesh, J. Stat. Mech. (2017) 113304.
[85] A. Gschwind, M. Klopotek, Y. Ai, and M. Oettel, Phys. Rev. E **96**, 012104 (2017).
[86] D. Nicholson and N. D. Parsonage, *Computer Simulation and the Statistical Mechanics of Adsorption* (Academic Press, London, 1982).
[87] K. Binder, *Applications of the Monte Carlo Method in Statistical Physics*, Topics in Current Physics (Springer, Berlin, 1984), Vol. 36.
[88] K. Binder, J. Stat. Phys. **24**, 69 (1981).
[89] T. L. Polgreen, Phys. Rev. B **29**, 1468 (1984).
[90] J. P. Hansen and L. Verlet, Phys. Rev. **184**, 151 (1969).
[91] W. H. Press, B. P. Flannery, S. A. Teukolsky, and W. T. Vetterling, *Numerical Recipes in C: The Art of Scientific Computing* (Cambridge University Press, Cambridge, 1992).
[92] A. J. Ramirez-Pastor, T. P. Eggarter, V. D. Pereyra, and J. L. Riccardo, Phys. Rev. B **59**, 11027 (1999).
[93] A. Ghosh, D. Dhar, and J. L. Jacobsen, Phys. Rev. E **75**, 011115 (2007).
[94] Available at http://cluster_infap.unsl.edu.ar/wordpress.